Effect of nano-Si_2O and nano-Al_2O_3 on cement mortars for use in agriculture and livestock production

Nestor León , Jordi Massana , Francisco Alonso , Amparo Moragues , Elvira Sánchez-Espinosa

The effect of nano-silica, nano-alumina and binary combinations on surface hardness, resistance to abrasion and freeze-thaw cycle resistance in cement mortars was investigated. The Vickers hardness, the Los Angeles coefficient (LA) and the loss of mass in each of the freeze–thaw cycles to which the samples were subjected were measured. Four cement mortars CEM I 52.5R were prepared, one as control, and the other three with the additions: 5% nano-Si, 5% nano-Al and mix 2.5% n-Si and 2.5% n-Al. Mortars were tested at 7, 28 and 90 d of curing to determine compression strength, total porosity and pore distribution by mercury intrusion porosimetry (MIP) and the relationship between the CSH gel and Portlandite total by thermal gravimetric analysis (TGA). The capillary suction coefficient and an analysis by a scanning electron microscope (SEM) was made. There was a large increase in Vickers surface hardness for 5% n-Si mortar and a slight increase in resistance to abrasion. No significant difference was found between the mortars with nano-particles, whose LA was about 10.8, classifying them as materials with good resistance to abrasion. The microstructure shows that the addition of n-Si in mortars refines their porous matrix, increases the amount of hydrated gels and generates significant changes in both Portlandite and Ettringite. This produced a significant improvement in freeze–thaw cycle resistance. The effect of n-Al on mortar was null or negative with respect to freeze–thaw cycle resistance.

Keywords:
Nano-Si
Nano-Al
Mortar
Surface hardness
Abrasion
Freeze–thaw cycles

1. Introduction

In rural areas, cement mortar and concrete, essential as construction materials, are used in many agriculture and livestock production facilities (Sánchez, Garcimartín, Jofré, & Burón, 2010). Their most frequent use is in the "in situ" manufacture of continuous floors and discontinuous precast floors. These floors can be both protected or outdoors, and therefore subject to environmental conditions of the

Nomenclature

ANOVA	analysis of variance
BSEM	back-scattering
Ca^{2+}	calcium ion [mol m^{-3}]
$Ca(OH)_2$	calcium hydroxide or portlandite
Cl^{-1}	chloride ion [mol m^{-3}]
CSH	calcium silicate hydrate
d	days
DTA	differential thermal analysis
h	hours
LA	Los Angeles
LSD	Fisher least significant differences procedure
MIP	porosimetry by mercury intrusion
MN	control mortar
M[nSi]	mortar in which 5% mass of cement was replaced by 5% of nSi
M[nAl]	mortar in which 5% mass of cement was replaced by 5% of nAl
M[nSi]:[nAl]	mortar in which 5% mass of cement was replaced by 2.5% nSi and 2.5% nAl
nano-Al_2O_3	nanoalumina
nano-SiO_2	nanosilica
nAl	nanoalumina
nSi	nanosilica
nSi–nAl	nanosilica and nanoalumina
NH^{+4}	ammonium [mol m^{-3}]
p	*p*-value
SE	means of secondary electrons
SEM	scanning electronic micrographs
SP	superplastifier additive
TGA	thermogravimetric analysis

operating farm and/or weather. In many cases good durability is required, although most buildings and rural facilities require no great mechanical strength.

The usually strength to satisfy the requirements of both on-site and prefabricated elements is about 30–35 MPa, but this is subject to corrosive chemical environments (acid media, and aggressive ions; Cl^{-1}, NH^{+4},...), physical wear (mainly abrasion by livestock hoofs or vehicle wheels) (Massana, Guerrero, Antón, Garcimartín, & Sánchez, 2013), as well as weather. Cement materials used in these environments should meet requirements of hardness, resistance to fracturing and abrasion and resistance to freeze thaw cycles. Failure to meet these requirements may result in such damage as loss of material and cracking. This impairment may increase the risk of reinforcement corrosion which can lead to partial or total collapse of structural elements, with the risk of interruption of production or damage to livestock, with consequent economic losses.

Addition of nano-particles to cement material has been of increasing interest in recent decades. Of the various nano-additions employed in civil engineering, most-used are silica, titanium, aluminium and iron nano-particles (Sánchez & Sobolev, 2010). The type of addition chosen depends on the properties to be improved or attained, related with the function to be developed (Schmidt et al., 2013). Most studies of nano-particles in concentrate on nano-SiO_2 (Kawashima, Hou, Corr, & Shah, 2013). Most of these studies found that nano-SiO_2 addition changes microstructures through the activation of pozzolanic reactions (Bjornstrom, Martinelli, Matic, Borjesson, & Panas, 2004; Jo, Kim, Tae, & Park, 2007). Similar to silica fume, nano-SiO_2 reacts with calcium hydroxide ($Ca(OH)_2$) to increase the amount of CSH gel, increasing material density while reducing permeability (Li, Zhang, & Ou, 2006) and controlling Ca^{2+} lixiviation (Schmidt et al., 2013; Zyganitidis, Stefanidou, Kalfagiannis, & Logothetidis, 2011). The size of the silica addition changes the average size and number of Portlandite crystals (Bjornstrom et al., 2004). These microstructural changes are associated with such microstructure properties, of both mortars and concretes, as strength and elastic module (Arefi et al., 2011; Byung-Wan, Chang-Hyun, Ghi-ho, & Jong-Bin, 2007; Mondal, Shah, Marks, & Gaitero, 2010; Schmidt et al., 2013; Singh, Agarwal, Bhattacharyya, Sharma, & Ahalawat, 2011), durability (Dolado et al., 2007; He & Shi, 2008; Zhang & Li, 2011), fatigue (Li, Zhang, & Ou, 2007), amongst others. Studies of the effects of nano-Al_2O_3 are relatively few, referring mainly to effects on mechanical properties, absorption of water permeability in mortars and concretes (Campillo et al., 2007; Li, Wang, He, Lu, & Wang, 2006; Li, Zhang, et al., 2006; Oltulu & Sahin, 2011, 2013). Nazari and Riahi (2011) studied abrasion resistance in concrete with nano-SiO_2 and nano-Al_2O_3. However there are very few studies about the effect of said additions on properties such as hardness, resistance to fracture and abrasion, and resistance to freeze–thaw cycles, in mortars used in agriculture or livestock.

The objective of this work was the study of the effect of nano-SiO_2, nano-Al_2O_3 and a binary combination of both additions on surface hardness, resistance to abrasion and resistance to freeze–thaw cycles of mortars and cement.

It is worth noting that in cement materials, mass loss of the surface depends on the matrix microstructure, the porosity and the degree of adherence of the aggregates to the matrix. Weakness in this area is determined by higher content of crystals with a surface/mass ratio a lot more unfavourable than hydrated cement gels. An improvement in the studied properties could produce a material more appropriate and sustainable for livestock facilities with a high degree of abrasion, caused by the hooves of animals and/or weather.

2. Materials and methods

Materials used were CEM I 52.5R cement (UNE-EN 197-1:2011). Two different oxides were added to the mixtures: nano-silica in 40% solution with a maximum particle size of 12 nm (Blaine value 200 $m^2\ g^{-1}$, distributed by Obermeier, Bad Berleburg, Germany), submicronic-powder of alumina with a particle size between 260 and 550 nm (Blaine value 9–7 $m^2\ g^{-1}$, distributed by Vicar S.A. Manises, Valencia, Spain). Also, a polycarboxylate as superplastifier additive (SP) (Viscocrete 5720 distributed by SIKA, Alcobendas, Madrid, Spain) was used, normalised sand CEN (UNE-EN 196-1, 2005) and drinking water. The chemical composition of cement is shown in Table 1.

The control mortar (MN) was prepared with a water/cement ratio of 0.47, and a ratio of cement/sand of 1/3 mass%,

Table 1 – Cement chemical composition (% mass).									
CaO	SiO_2	Al_2O_3	Fe_2O_3	MgO	K_2O	SO_3	Cl^-	Na_2O	I.L.
63.41	19.2	6.07	1.7	2.56	0.82	3.38	–	0.33	2.09

as specified in the European standard EN 196-1:2005 (thus 450 g cement and 1350 g of sand per mould). In the other three mortars 5% by mass of cement was replaced by 5% of nano-SiO_2 (M[nSi]), 5% nano-Al_2O_3 (M[nAl]) and 2.5% nSi and 2.5% nAl (M[nSi]:[nAl]), respectively (water/binder ratio of 0.47). In these mortars with nano-additions was added 1.2% of SP versus cement weight.

To test surface hardness and abrasion resistance, 20 samples of 40 × 40 × 160 mm of each mortar type were prepared. Samples removed from moulds after 24 h and submerged in water in a chamber at 20 ± 2 °C. Twenty-eight days after production, 11 samples of each mortar were cut into four 40 × 40 × 40 mm cubes. Of these 44 cubes per mortar type, 2 were chosen at random for the measurement of capillary absorption of water (UNE 83982:2008). Another 4 cubes were tested with a Brinell universal hardness meter at Hd 2.5/62.5/30 and Hd 2.5/187/30 for their Vickers hardness (EN ISO 6506-4:2007), by conversion of the results obtained. The cut surface of each sample was tested at 20 points at least 2 mm apart. Afterwards the Los Angeles test was done. The LA coefficient was determined according to UNE-10972:2010, specifically for aggregates. As a reference thirty 40 × 40 × 40 mm granite cubes, were measured for their Vickers hardness and LA coefficient.

Of the remaining 9 samples, 2 were tested for compression strength at 7, 28 and 90 d according to UNE-EN 196-1, 2005. The rest of samples (one for each mortar) were studied to determinate their microstructure. For each sample the porosimetry by mercury intrusion (MIP) was analysed (by extraction of three cylinders each samples) according to ASTM D4404-84:2004; the water loss by thermogravimetric analysis (TGA) and differential thermal analysis (DTA) (by extraction of two slices in different positions from each specimen) according to ASTM E1131:2008. From the DTA results, temperatures at were recorded at the start and end of each of the intervals corresponding to the water loss. Finally mortars were studied by scanning electronic micrographs (SEM), by preparation and analysis of four specimens (two of the central area and two in the outermost portion of the specimen) for each mortar sample.

The porosity test (MIP) was carried out with a Micromeritics device, model Autopore IV 9500 (Bonsai Advanced Technologies, Alcobendas Spain) under a maximum pressure of 227.5 MPa, covering a range of pores from 5 nm to 180 μm, with 3 ± 0.01 g samples stabilised at 40 °C to a constant weight. Testing evaluated porosity, pore-size distribution and pore volume for each mortar and age studied.

Table 2 – Least squares for Vickers hardness.		
Mortars	Vickers hardness	sem
MN	53.44[a]	2.48
M[nSi]	77.34[b]	
M[nAl]	70.51[c]	
M[nSi]:[nAl]	65.46[c]	

[a,b,c]Mean with different superscript, the differences are statistically significant ($p < 0.05$) LSD – 95%. sem is the standard error of the mean.

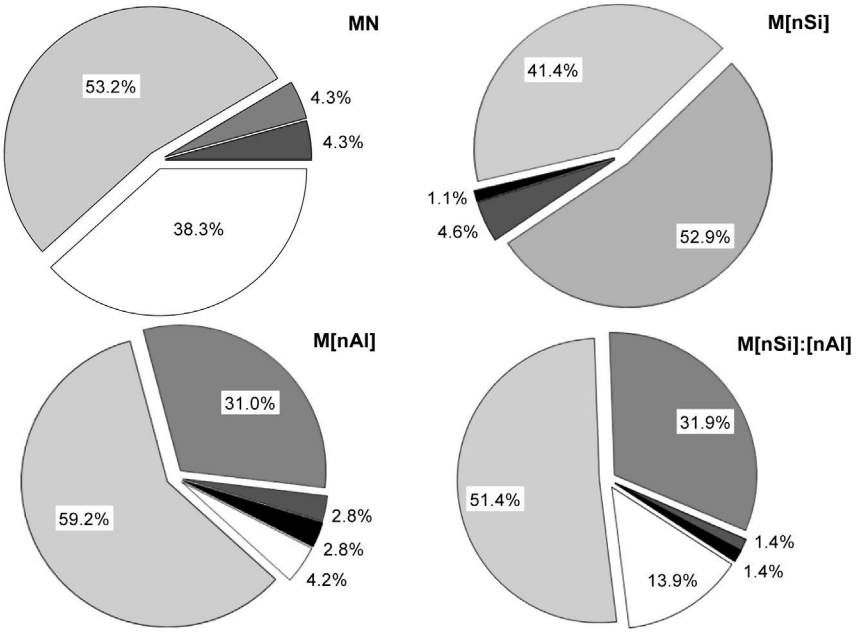

Fig. 1 – Percentage distribution of Vickers hardness intervals.

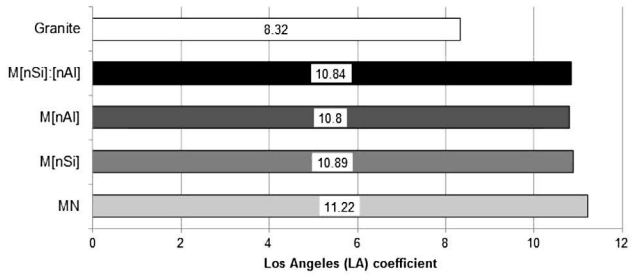

Fig. 2 – Los Angeles (LA) coefficients.

A Evo Labsys Setaram (Bonsai Advanced Technologies, Alcobendas, Spain) simultaneous thermal analyses, was used for the thermal gravimetric analysis, TGA, with a precision of 0.1 μg, a rate of heating of 10 °C min^{-1}, in a nitrogen atmosphere to determine the amount of CSH gel and Portlandite ($Ca(OH)_2$) in each mortar.

Micrographs were produced in an Oxford Instruments JEOL JSM 6335F Scanning Electron Microscope (SEM) with an X–ray analysis of dispersive energy. The device is equipped with an 80 mm^2 X-MAX model with a 127 eV at 5.9 KeV resolution, producing images by means of secondary electrons (SE) and back-scattering (BSEM).

To test freeze–thaw cycle resistance, six samples of 150 × 150 × 75 mm were made, removed from moulds after 24 h and tested according to UNE-CEN/TS 12390 EX: 2008.

Compressive strength, hardness and mass loss data were statistically analyses by an analysis of variance with the StatGraphics v.5.1 (2002) program (Pearson Educación S.A., Madrid, Spain). The discriminate used for averages was the Fisher least significant differences procedure (LSD) with $p < 0.05$.

3. Results

3.1. *Surface hardness*

The surface of any material made up from different minerals (rocks) or different materials (mortars and concrete) varies in hardness according to the point of measurement on the surface. Mortar can be considered to be a two-phase material: aggregates and hydrated cement matrix. Table 2 shows the average values and results of the variance in the Vickers hardness.

The average value (77.34) of the Vickers hardness of M[nSi] was significantly greater than that of the other mortars.

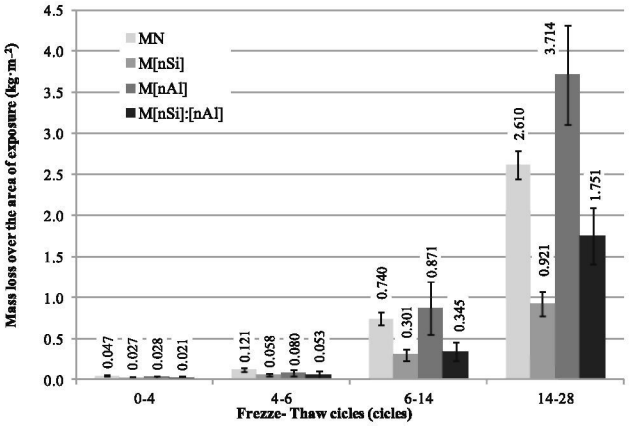

Fig. 4 – Loss of mass relative to the area exposed (kg m^{-2}) in each freeze–thaw cycle.

Addition of 5% nSi increases hardness by 45%. Addition of nAl yields an increase of 31%; addition of nSi–nAl yields an increase of 22%. The hardness of the two latter mortars was not significantly different. They were, however, significantly harder than the control mortar. The variation in hardness values of a sample, a reflection of its multiphase nature, can be illustrative when shown in detail, as plotted in Fig. 1 for groups of Vickers hardness measurements falling into intervals: <48, 49–69, 70–99, 100–129, >130. Vickers hardness was measured on the cut surface of the mortars. Repetition of measurement ensured that the hardness meter tested aggregates an equal number of times for each of the samples.

Figure 1 shows a significant change in percentage of each of the hardness intervals. Addition of 5% nSi eliminates the <48 interval, while hardness measurement of 70–99 account for 53% of results, while the 49–69 hardness interval is reduced to 41%, from the 53% of the control mortar surface. Vickers hardness also is increased by the nAl addition, but in a smaller proportion. The <48 interval accounts for 39% of measurement for the MN mortar, but only 4% and 14% for the M[nAl] and M[nSi]:M[nAl], respectively. Furthermore the 70–99 interval increases to 31% and 32% for the M[nAl] and M[nSi]:M[nAl], respectively, from 4% for the MN.

3.2. *Resistance to abrasion*

Although not commonly used, the LA coefficient was measured to determine resistance to abrasion. This test (UNE-10972:2010) is required to determine the suitability of aggregates (EHE, 2010) and provides a measure of the cohesion of

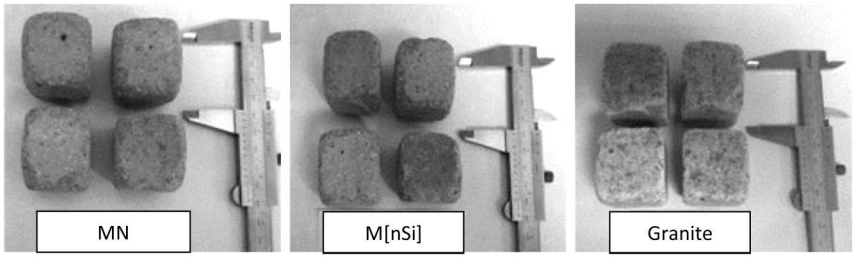

Fig. 3 – MN, M[nSi] and granite samples after Los Angeles testing.

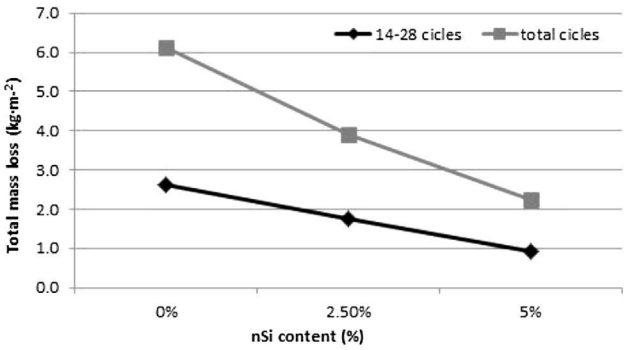

Fig. 5 – Loss of mass relative to the area exposed (kg m^{-2}) vs. percentage of nSi.

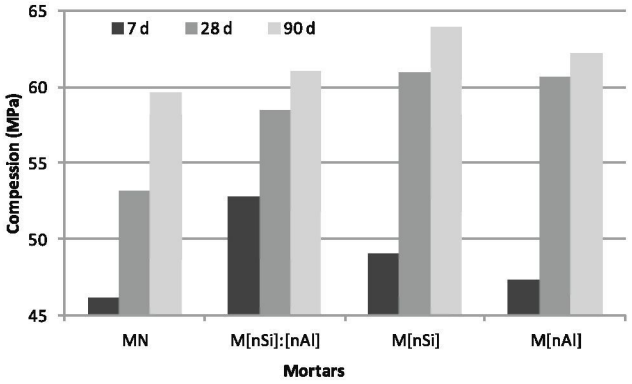

Fig. 6 – Evolution of the compressive strength of mortars at 7, 28 and 90 d of curing.

the constituents of a material. Aggregates with ratios <20 are considered materials with very good resistance to abrasion (Férnandez Cánovas, 2013). Figure 2 shows the LA coefficients obtained.

There were significant differences between the coefficients of Los Angeles of mortars and granite; this ratio was 24% less for granite compared with the mean value of the coefficients of mortars. When comparing only the LA coefficients of all mortars checked, using analysis of variance (ANOVA), there were significant differences between mortars with additions and the reference mortar. During the test it was observed that none of the pieces of mortar fragmented, and abrasion was located in the corners of the cube (see Fig. 3). However, about 53% of the pieces of granite fragmented, although this did not affect the LA coefficient because the fragments had their granulometric fractions set by the standard. These results highlight the potential influence of defects, cracks and load when natural materials are used.

Table 3 – Least squares means of compressive strength.

Level	Count	Mean (MPa)	sem
Mortar type			
MN	12	52.97^{a}	0.76
M[nAl]	12	56.71^{b}	
M[nSi]	12	57.92^{b}	
M[nSi]:[nAl]	12	57.42^{b}	
Time (d)			
7	16	48.81^{a}	0.66
28	16	58.28^{b}	
90	16	61.67^{c}	
Mortar by time			
MN-7	4	46.09^{a}	1.32
MN-28	4	53.12^{b}	
MN-90	4	59.69^{c}	
M[nAl]-7	4	47.28^{a}	
M[nAl]-28	4	60.63^{c}	
M[nAl]-90	4	62.23^{c}	
M[nSi]-7	4	49.07^{a}	
M[nSi]-28	4	60.94^{c}	
M[nSi]-90	4	63.75^{c}	
M[nSi]:[nAl]-7	4	52.81^{b}	
M[nSi]:[nAl]-28	4	58.44^{c}	
M[nSi]:[nAl]-90	4	61.00^{c}	

^{a,b,c}Means with different superscript showing statistically significant differences ($p < 0.05$) LSD – 95%.
N = Number of observations; sem: Standard error of the mean.

3.3. *Resistance to freeze–thaw cycles*

Figure 4 shows the mean and standard deviation of the results obtained in the freeze–thaw testing.

Figure 4 shows that until the sixth cycle there were no significant differences in mass loss among the mortars tested. However, at the end of cycle 14 mortars MN and M[nAl] did not show significant differences, but there are differences with respect to mortars with nano-SiO_2. After 28 cycles there were significant differences among all the mortars.

Mortar M[nSi] resists freeze–thaw cycles significantly better than the others, while mortar M[nAl] resists the least. For M[nSi], mass loss after 28 cycles is similar to the loss of mass of M[nAl] after only half the number of cycles. So the freeze–thaw cycle resistance of M[nSi] is 75% greater than that of M[nAl], 50% greater than that of M[nSi]:[nAl] and 30% greater than that of MN. The improvement due to nano-SiO_2 is proportional to the percentage of addition used, regardless of the presence of another addition. This proportionality is maintained both for the mass loss of the sample in the last freeze–thaw cycle as for total cycles (see Fig. 5).

3.4. *Compressive strength*

Table 3 shows ANOVA of the test of compressive strength for mortar type, time and their interaction. Figure 6 shows the compressive strength values at 7, 28 and 90 d of curing.

The average compressive strength of the reference mortar shows significant differences with respect to the average compressive strength of the mortars with nano-additions. These average values are Fig. 1 similar to each other and superior to those obtained in mortar MN. However, as expected, there are significant differences between times, with an increase until 90 d of curing. It is noteworthy that in all mortars with nano-additions, the values of compressive strength at 28 and 90 d of curing were similar, being significantly different with respect to the control mortar.

Although the addition of nano-particles results an increase in the average value of compressive strength, this was not

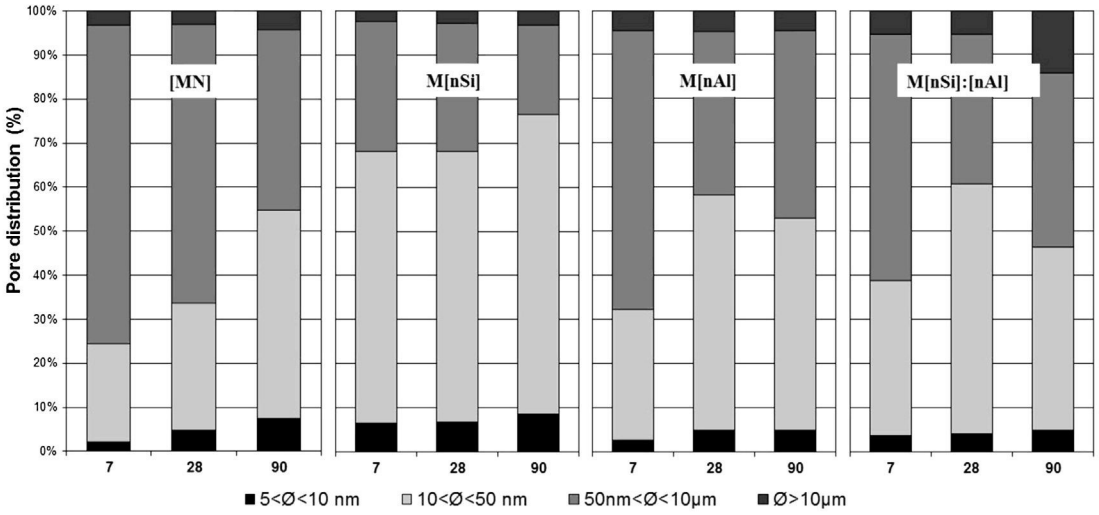

Fig. 7 – Pore-size distribution of mortar at 7, 28 and 90 d of curing according to the Mindess et al. (2003) classification.

very high, being 7% in mortar M[nAl], 9% in M[nSi] and 8% in M [nSi]:[nAl] with respect to the average value of the reference mortar at 28 d of curing.

3.5. *Mercury porosimetry intrusion*

The distribution of pore size was studied using the limits of the Mindess, Young, and Darwin (2003) classification. The four pore-size ranges established were: macro pores ($Ø > 10$ μm); large capillary (50 nm $< Ø <$ 10 μm); medium-size capillary (10 nm $< Ø <$ 50 nm) and small capillary (5 nm $< Ø <$ 10 nm). Figure 7 shows pore-size distribution for the 4 mortars at 7, 28 and 90 d of curing; Table 4 presents the percentage values of the pore size distribution after 28 d of curing.

In Fig. 7 a normal progressive refinement of the porous structure in the mortar without additions is observed. This is due to the reactions of cement hydration. However, in the mortar with only nano-Si there were no differences in the distribution of the pores between 7 and 28 d of curing.

Table 4 – Percentage values of pore-size distribution after 28 d.

Interval Ø pore	MN	M[nSi]	M[nAl]	M[nSi]:[nAl]
5 < Ø < 10 nm	5	7	5	4
10 < Ø < 50 nm	29	61	53	56
50 nm < Ø < 10 μm	63	29	37	34
Ø > 10 μm	3	3	5	5
TOTAL	100	100	100	100

So at 7 d the percentage of large capillaries, between 50 nm and 10 μm, for mortar M[nSi] is 29% (equal to the percentage at 28 d of curing) versus 72% for MN, 63% for M [nAl] and 56% for M[nSi]:[nAl]. After 28 d (Table 4) the percentage of pores of diameter 10–50 nm for MN mortar was 29%, significantly lower than in the other mortars with 61%, 53% and 56% for M[nSi], M[nAl] and M[nSi]:[nAl] respectively.

In the two mortars with nano-Al the pore size distribution was similar (Table 4). There was a significant increase in the percentage of pores between 10 nm and 50 nm in diameter at 28 d of curing and a reduction this percentage at 90 d. Both values were similar to the mortar MN at the same age. Table 5 shows total porosity and critical pore size for the mortars tested at 28 d of curing.

In Table 5, mortar M[nSi] shows the lower critical pore size and total porosity of the all mortars. The highest values were for control mortar MN, while intermediate values were obtained for the other two mortars. It should be noted that in nano-Al mortars critical pore size values were similar at 7 and 28 d. This also occurs with the values of total porosity, although they were slightly higher in mortar M[nAl]. However, this is reversed at 90 d of curing. The presence of macro pores (possibly due to a compacting and homogenisation of mixture) in samples containing nano-Al_2O_3 can reach higher than expected values of total porosity. This may be the reason for the high porosity of mortar M[nSi]:[nAl] at 90 d. However, the critical pore size shows the refinement of the porous structure associated with the addition.

Table 5 – Critical pore size and total porosity of mortars tested.

d	MN		M[nSi]		M[nAl]		M[nSi]:[nAl]	
	Critical	Total	Critical	Total	Critical	Total	Critical	Total
7	0.062	14.29	0.027	12.07	0.040	13.05	0.050	12.87
28	0.052	13.25	0.021	11.56	0.032	12.91	0.032	12.12
90	0.040	12.46	0.021	10.79	0.040	12.10	0.032	13.46

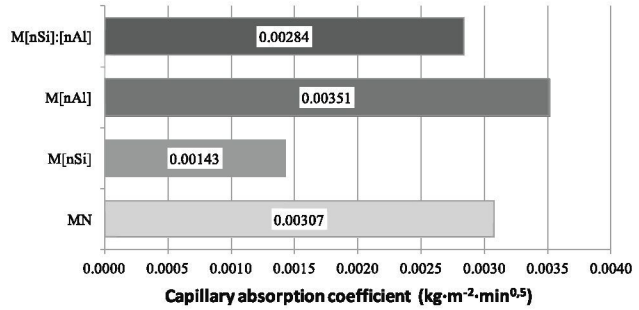

Fig. 8 – Capillary absorption coefficients for mortars studied.

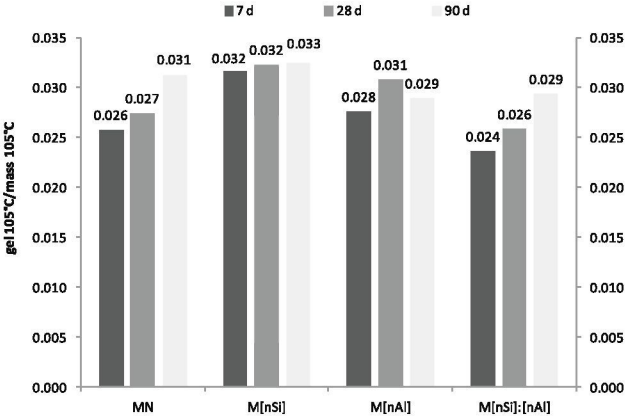

Fig. 9 – Thermal gravimetric analysis results and CSH water loss with respect to sample mass at 105 °C.

3.6. *Capillary absorption coefficient*

Figure 8 shows the capillary absorption coefficients obtained for the mortars studied.

It can be seen in Fig. 8 that the greatest capillary absorption coefficient corresponds to mortar M[nAl] (0.0035), reduced by 13% in the case of control mortar MN (0.0030). The 0.0028 capillary absorption coefficient for M[nSi]:[nAl] is 20% smaller than that of M[nAl]. The smallest coefficient, 0.0014, corresponds to M[nSi], 50% smaller than that of M[nAl].

3.7. *Thermal gravimetric analysis*

Water loss between 105 °C and 400–450 °C of temperatures was used to calculate CSH gel percentages. The percentage of $Ca(OH)_2$ was calculated between 400–450 °C and 500–550 °C (Rivera Lozano, 2004). The exact limits of temperature for each sample were defined from DTA. Table 6 shows the thermal gravimetric analysis (TGA) results obtained for samples studied.

Figures 9 and 10 show the relation between gel water loss and Portlandite water loss with respect to sample mass at 105 °C.

Figure 9 shows that higher values, and therefore the greatest amount, of CSH gel are obtained in M[nSi] at all ages. Mortar M[nSi]:[nAl] is the one with lowest values. In Fig. 10, shows that the same mortar, M[nSi], has the smallest losses of Portlandite free water. It should be noted that mortar M[nAl] is the one with the maximum values of free Portlandite at all ages.

Figure 11 shows the variations in total Portlandite water of the different samples studied. The total loss of mass corresponding to total Portlandite is calculated by adding to the free Portlandite loss the 41% of mass loss from the decarbonation interval corresponding to a range between 550 °C and 1110 °C.

In Fig. 12 the relation between loss of CSH gel and loss of Portlandite can be seen.

Figure 12 shows that in the case of M[nSi] this relationship reaches its highest values, due both to the increase in gel and reduction in Portlandite. In mortars M[nAl], this relationship is lower with respect to the MN and mortars and M[nSi]:[nAl], except at 7 d when it is higher with respect to the same mortars. The amount of Portlandite increased in this mortar, but the gel was not so active as in the mortar MN. M[nSi]:[nAl] sample relationships were similar to those obtained for mortar MN, but with slightly higher values at 28 and 90 d. In all cases hydration occurred more intensely between 7 and 28 d, as shown by the change in slope of the graphs shown in Fig. 12.

3.8. *Scanning Electron Microscope*

Figure 13 shows the micrographs of mortars studied at 28 d, where morphological differences in crystals precipitated in the inside of the pores of the different mortars can be observed.

In mortar MN a large amount of Portlandite of varied morphology can be seen. Additions of nSi and nAl particles create differences in the microstructure of hardened pastes. In the mortar M[nSi] deformed Portlandite can be seen that is similar to that found by other authors (Byung-Wan et al., 2007; Qing, Zenan, Deyu, & Rongshen, 2007) with similar dosages. However, in mortar M[nAl] a significant number of crystals of Portlandite in the form of plates or with hexagonal morphology can be seen. Finally, in the micrograph of mortar M[nSi]:[nAl], crystals of Portlandite of both morphologies and

Table 6 – Thermal gravimetric analysis (TGA).

Mortar	MN			M[nSi]			M[nAl]			M[nSi]:[nAl]		
Time (days)	7	28	90	7	28	90	7	28	90	7	28	90
Sample mass 105 °C	54.904	56.176	55.977	59.445	59.217	59.315	55.095	53.877	54.875	56.014	55.118	54.919
CSH water 105 °C	1.415	1.541	1.754	1.878	1.912	1.928	1.520	1.659	1.587	1.323	1.424	1.612
Free $Ca(OH)_2$ water	0.759	0.719	0.804	0.652	0.7	0.699	0.787	0.832	0.781	0.632	0.678	0.794
CO_2	1.121	1.28	1.385	1.498	1.199	1.119	1.211	1.271	1.42	1.246	1.091	1.062
Total Portlandite	1.219	1.244	1.372	1.266	1.192	1.158	1.284	1.353	1.363	1.143	1.125	1.229

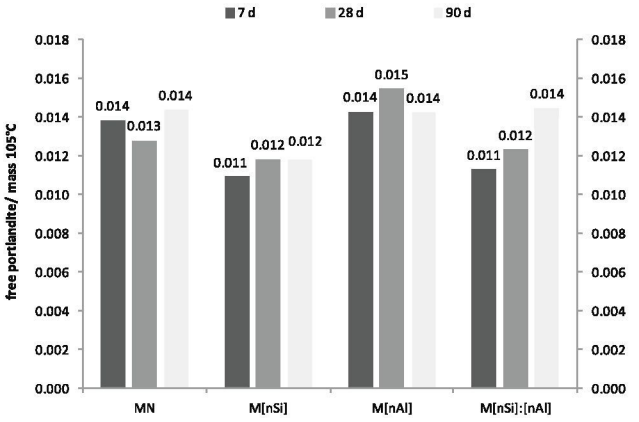

Fig. 10 – Thermal gravimetric analysis results: free Portlandite water loss with respect to sample mass at 105 °C.

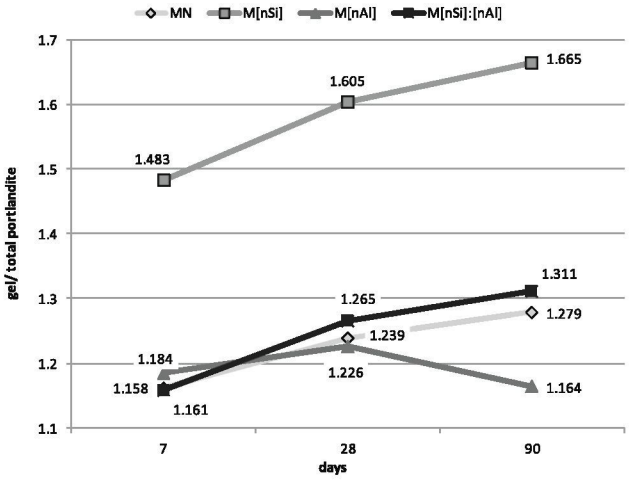

Fig. 12 – Relation between CSH gel loss and total Portlandite loss.

Ettringite are distributed haphazardly. Both results produced a less compact microstructure than that of the mortar with only nano-SiO_2. It is noteworthy that whenever nano-SiO_2 has been added a small proportion of Ettringite is maintained at long ages.

4. Discussion

Analysis of results shows that mortars with nano-SiO_2, nano-Al_2O_3 or both additions improved surface hardness and abrasion resistance. This result agrees with that obtained by Naza and Riahi (2011). They studied abrasion resistance by determining the depth of wear (ASTM C1138) in concrete with nano-SiO_2, nano-Al_2O_3, in two different curing media. They conclude that in both media, wear resistance is enhanced by increasing the content of nanoparticles, and even more in mortars with nano-SiO_2. Besides these authors, Oltulu and Sahin (2013) considered that wear resistance is associated with the compressive strength of mortars studied, although not exclusively. Thus, analysis of changes in the ranges of different mortar surface hardness shows that the matrix hardens, possibly associated with changes in the microstructure of the matrix.

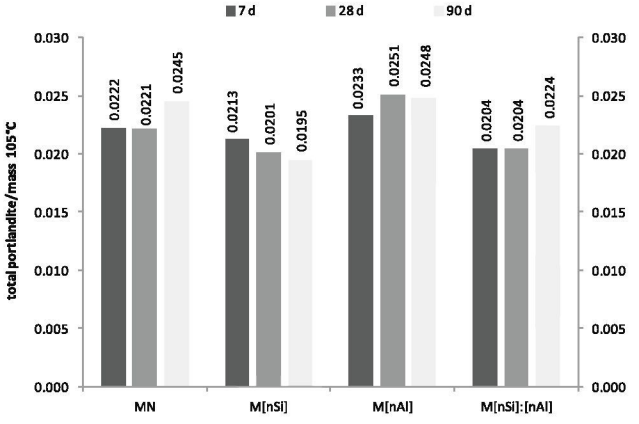

Fig. 11 – Variation in total Portlandite water in the various samples studied.

Analysis of results of microstructural characterisation shows that, in general, there is a decrease in total porosity and critical pore diameter with respect to the reference mortar MN. These variations occur associated with a change in the pore size distribution, with increased medium pore and decreased large pores capillary. Although this can be seen in all mortars, values are significantly lower in the case of mortar M[nSi].

Variations in total porosity versus curing time show that progression of the hydration process closes porous structure. This decreases the values of total porosity (Gaitero, Campillo, & Guerrero, 2008). Incorporation of nano-SiO_2 affects the critical pore size, significantly reducing values from 0.062 to 0.021 μm with 28 d of curing.

The percentage distribution of the different pore sizes of two samples containing nano-Al_2O_3 is practically similar. Total porosity and critical pore radius values are not reduced significantly compared with mortar without addition. In these samples the number of macro-pores is greater than in the reference. This may be caused by the great difficulty of homogenisation and dispersion of nano-powders in the mixtures. However, macroscopic behaviour is not practically affected, but microstructure is affected and hence the durability.

Analysis of the mass loss of mortar under freeze–thaw cycles shows a direct relationship between this coefficient and capillary suction. In this study the mortar with 5% nano-Al_2O_3 has the highest coefficient of capillary suction and greater mass loss in freeze–thaw cycles. These results contradict those obtained by Oltulu and Sahin (2011) in which the addition of 1.25% of nano-Al_2O_3 powder in mortar produced the best compressive strength and capillary permeability after 180th day of curing. Certainly these results are not comparable with ours. On the one hand mortar they used contained silica fume while ours were made with Portland cement (OPC). Moreover the percentages of nano-addition were different. The same applies to results obtained by the same authors in another paper (Oltulu & Sahin, 2013) from cement mortar containing fly ash. In this study, the mortar with nano-SiO_2

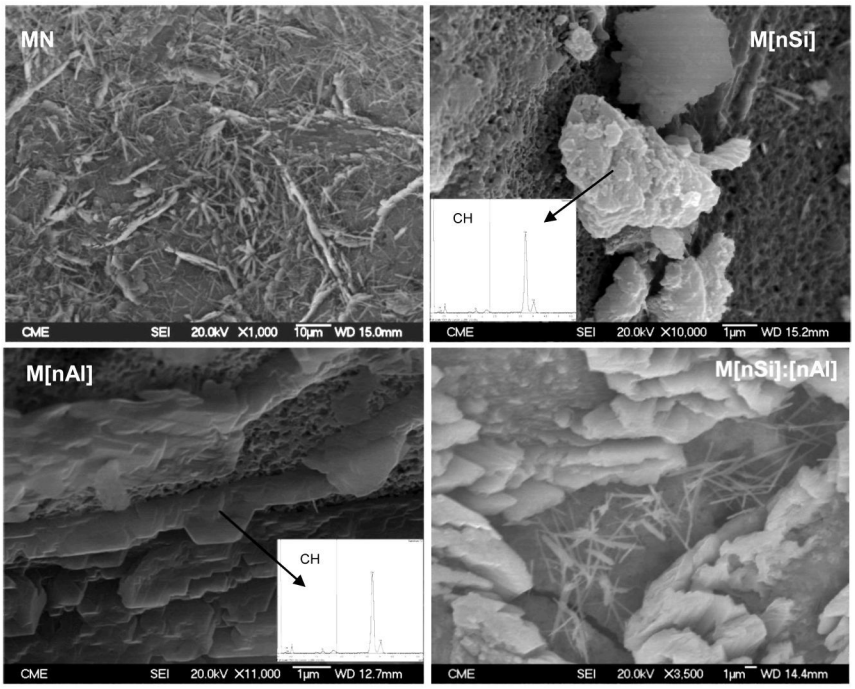

Fig. 13 – Scanning Electron Microscope micrographs of the mortars studied.

had the lowest coefficient of capillary suction but the percentage of nano-addition replacement of cement was 1.25%, corresponding to the mortar with 2.5% nano-SiO_2 and the highest coefficient.

However, although the cements were different, this is not the most significant difference between the mortars with nano-alumina. The greatest difference is in particle size and presentation (Sánchez & Sobolev, 2010). Thus Oltulu and Sahin use nano-Al_2O_3 with a maximum particle size of 13 nm, while in this study nano-particle size was between 260 and 550 nm. This agrees with Gaitero et al. (2008), who claim that the beneficial effects depend on the presentation of the nanoparticle, being higher in the colloidal dispersions than in dry ones, as in our case (Campillo et al., 2007; Quercia, Spiesz, Hüskenc, & Brouwers, 2014).

Also TGA results confirm this behaviour. So mortar M[nAl] has a lower gel/total Portlandite relationship, except at 7 d of curing, followed by reference mortar MN and M[nSi]:[nAl]. This could indicate that nano-Al_2O_3 accelerates hydration reactions in the early ages (Campillo et al., 2007) but does not interfere with the pozzolanic reaction of silica. However the relationship of gel/total Portlandite in mortar M[nSi] reaches very high values. This is because of high CSH gel content and small amounts of Portlandite. This result agrees with those presented by other authors (Arefi et al., 2011; Byung-Wan et al., 2007; Kong et al., 2012; Nazari and Riahi, 2011). The mechanism can be summarised as starting with the formation of $Ca(OH)_2$ produced by the reactions of hydration of cement and water. Nano-SiO_2 activity is high due to a large specific surface and quick reaction with $Ca(OH)_2$. In this reaction CSH occurs again and therefore the amount of $Ca(OH)_2$ is reduced. The CSH gel fills voids and improves the density of the cement matrix (Ji, 2005).

These changes in microstructure were reflected in the compressive strength of mortars studied. As expected mortar M[nSi] had greater compressive strength at 28 and 90 d. However, an ANOVA shows no significant difference between these values and those for mortars with nano-particles, but does differ significantly from the value for the reference mortar at 28 d. These increases in compression strength (7% in M[nAl]; 9% in M[nSi] and 8% in M[nSi]:[nAl]) with respect to the average reference mortar value are slightly smaller than those obtained by other researchers (Najigivi, Khaloo, Iraji zad, & Abdul Rashid, 2013; Singh et al., 2011; Zyganitidis et al., 2011). With the same percentage of nano-Si_2O Li, Wang, et al. (2006), Li, Zhang, et al. (2006) obtained an increase in strength of 14% at 28 d.

There are a number of studies than conclude that the optimal amounts of nano-Si_2O must be less than 4% mass (Nazari & Riahi, 2010, 2011), or even lower values of 2% mass (Najigivi et al., 2013; Nazar and Riahi, 2011; Oltulu & Sahin, 2013). However Senff, Hotza, Repette, Ferreira, and Labrincha (2010) has excellent compression strength results with percentages of cement replacement by nano-Si_2O 7% mass and Li et al. (2006) of 10% mass. In both studies SP was used in the mixture. Also Fernández et al. (2013) used SP with 6% mass to obtain mixtures that quadrupled the compressive strength of the control mortar at 182 d of curing.

The lower compressive strength value may be due to the size of the nano-Si_2O (12 nm) used in our work. Haruehansapong, Pulngern, and Chucheepsakul (2014) found that sizes from 12 nm to 20 nm increased compressive strength, but less so than Si_2O with nano-particle size of 40 nm. The results obtained by these authors, in cement mortars with nano-Si_2O with a particle size of 12 nm, were similar to those obtained in our study. Furthermore, in this

paper, the percentage of cement replacement by nano-Si_2O is 5% mass and 2.5% mass, far lower than the 9% mass optimal replacement in the aforementioned work. As for mortars with nano-Al_2O_3 single, compressive strength results are lower than in the other mortars with nano-particles. This is consistent, although to a lesser extent, with the results obtained by Li, Wang, et al. (2006), Li, Zhang, et al. (2006). The authors believe it is due to inefficient distribution of nano-alumina powder in agreement with Quercia et al. (2014).

5. Conclusions

Results obtained herein permit one to affirm that nano-SiO_2, nano-Al_2O_3 and their binary combination, increase surface hardness as well as abrasion and fracture resistance, with significant changes in the matrix microstructure. The Vickers hardness values of rocks, e.g. basalt (132), are not very different from those obtained for the mortars used in this study. Optimisation of dosage or simple treatments like carbonation, could approximate the material behaviour of natural stone.

The mortars studied show an improvement in compression strength with respect to the control mortar, although compression strength values of the mortars studied are not significantly different. Mortars with nano-additions have LA coefficient values that classify them as a good material resistant to abrasion and fracture.

Microstructural characterisation allows us to affirm that improvement in the studied properties is associated with a refinement of the porous structure, a reduction in matrix total porosity and in critical pore diameter. With respect to the reference mortar there was modification in the pore size distribution, with increased medium-size capillary pores (10-50 nm) and a decrease in large capillary pores (50 nm–10 μm). The reduced workability of nano-Al_2O_3 samples could reasonably be the cause of the increase in macro pores (>10 μm).

In mortars with nano-SiO_2 the amount of CSH gel is increased while Portlandite is decreased due to pozzolanic activity. There is additionally an increase in the degree of cement hydration. Nevertheless, mortars with nano-Al_2O_3 show a relation between CSH gel loss and $Ca(OH)_2$ loss that is smaller than that of the control mortar. This indicates that gels formed in the presence of alumina undergo changes in stoichiometry, without consuming the Portlandite generated in any secondary reaction.

Addition of 5% of nano-SiO_2 produces a mortar M[nSi] with notably improved freeze–thaw cycle behaviour, while the effect of nano-Al_2O_3 addition is null or negative. The combination of both additions leads to an intermediate resistance, between the resistances produced by individual additions, but greater than that of the control mortar. Capillary water absorption is inversely related to the resistance to freeze-thaw cycles. So, the higher the water absorption coefficient by capillarity, the higher the mass losses of the samples, and therefore the less the resistance to freeze–thaw cycles. Cement replacement by 5% wt. of nano-Si_2O doubles mortar resistance to freeze–thaw cycles compared with the reference mortar.

In summary, the use of mortars containing 5% wt. of nano-Si_2O can be suitable for use in agriculture and livestock production. Since this represents an improvement of surface hardness, abrasion resistance and resistance to freeze–thaw cycles that is often needed. However, the percentage and size of replacement of the nano-particle should be optimised to achieve the required performance in accordance with the use and aggressiveness of the environment.

Acknowledgements

The authors are grateful for financial support from the Ministerio de Ciencia y Tecnología, project BIA2009-14395-C04-04 and from the Ministerio de Fomento, projects C14/2006 and C01/2007.

REFERENCES

Arefi, M. R., Javaheri, M. R., Mollaahmadi, E., Zare, H., Abdollahi Nejand, B., & Eskandari, M. (2011). Silica nanoparticle size effect on mechanical properties and microstructure of cement mortar. *Journal of American Science, 7*(10).

ASTM C1138. (1997). *Standard test method for abrasion resistance of concrete* (Underwater Method). ASTM International, USA: American Society for Testing and Materials.

ASTM D4404-84. (2004). *Standard test method for determination of pore volume and pore volume distribution of soil and rock by mercury intrusion porosimetry*. ASTM International, USA: American Society for Testing and Materials.

ASTM E1131. (2008). *Standard test method for compositional analysis by thermogravimetry*. ASTM International, USA: American Society for Testing and Materials.

Bjornstrom, J., Martinelli, A., Matic, A., Borjesson, L., & Panas, I. (2004). Accelerating effects of colloidal nano-silica for beneficial calcium–silica–hydrate formation in cement. *Chemical Physics Letters, 392*(1–3), 242–248.

Byung-Wan, J., Chang-Hyun, K., Ghi-ho, T., & Jong-Bin, P. (2007). Characteristics of cement mortar with nano-SiO_2 particles. *Construction and Building Materials, 21*, 1351–1355.

Campillo, I., Guerrero, A., Dolado, J. S., Porro, A., Ibáñez, J. A., & Goñi, S. (2007). Improve of initial mechanical strength by nano-alumina in belite cements. *Materials Letters, 61*(8–9), 1889–1892.

Dolado, J. S., Campillo, I., Erkizia, E., Ibáñez, J. A., Porro, A., Guerrero, A., et al. (2007). Effect of nanosilica additions on belite cement pastes held in sulphate solutions. *Journal of the American Ceramic Society, 90*(12), 3973–3976.

EHE Instrucción del hormigón Estructural. (2010). *Serie Normativa*. Secretaría General Técnica (4th ed.). Madrid. Spain: Ministerio de Fomento.

EN ISO 6506-4:2007. (2007). *Materiales metálicos. Ensayo de dureza Brinell. Parte 4: Tabla de valores de dureza*. Madrid. Spain: Asociación Española de Normalización y Certificación (AENOR).

Fernández, J. M., Durán, A., Navarro-Blasco, I., Lanas, J., Sirera, R., & Álvarez, J. I. (2013). Influence of nanosilica and a polycarboxylate ether superplasticizer on the performance of lime mortars. *Cement and Concrete Research, 43*, 12–24.

Fernández Cánovas, M. (2013). *Hormigón* (10th ed.). Madrid. Spain: Colegio de Ingenieros de Caminos, Canales y Puertos.

Gaitero, J. J., Campillo, I., & Guerrero, A. (2008). Reduction of the calcium leaching rate of cement paste by addition of silica nanoparticles. *Cement and Concrete Composite, 38*, 1112–1118.

Haruehansapong, S., Pulngern, T., & Chucheepsakul, S. (2014). Effect of the particle size of nanosilica on the compressive strength and the optimum replacement content of cement mortar containing nano-SiO_2. *Construction and Building Materials, 50*, 471–477.

He, X., & Shi, X. (2008). Chloride permeability and microstructure of Portland cement mortars incorporating nanomaterials. *Transportation Research Record: Journal of the Transportation Research Board*, 13–21.

Ji, T. (2005). Preliminary study on the water permeability and microstructure of concrete incorporating nano-Si_2O. *Cement and Concrete Research, 35*, 1943–1947.

Jo, B.-W., Kim, C.-H., Tae, G.-H., & Park, J.-B. (2007). Characteristics of cement mortar with nano-SiO_2 particles. *Construction and Building Materials, 21*, 1351–1355.

Kawashima, S., Hou, P., Corr, D. J., & Shah, S. P. (2013). Modification of cement-based materials with nanoparticles. *Cement and Concrete Composite, 36*, 8–15.

Kong, D., Du, X., Wei, S., Zhang, H., Yang, Y., & Shah, S. P. (2012). Influence of nano-silica agglomeration on microstructure and properties of the hardened cement-based materials. *Construction and Building Materials, 37*, 707–715.

Li, Z., Wang, H., He, S., Lu, Y., & Wang, M. (2006). Investigations on the preparation and mechanical properties of the nano-alumina reinforced cement composite. *Materials Letters, 60*(3), 356–359.

Li, H., Zhang, M.-H., & Ou, J.-P. (2006). Abrasion resistance of concrete containing nano-particles for pavement. *Wear, 260*(11–12), 1262–1266.

Li, H., Zhang, M.-H., & Ou, J.-P. (2007). Flexural fatigue performance of concrete containing nano-particles for pavement. *International Journal of Fatigue, 29*(7), 1292–1301.

Massana, J., Guerrero, A., Antón, R., Garcimartín, M. A., & Sánchez, E. (2013). The aggressiveness of pig slurry to cement mortars. *Biosystems Engineering, 114*, 124–134.

Mindess, S., Young, J. F., & Darwin, D. (2003). *Concrete* (2nd ed.). Upper Saddle River, NJ 07458: Prentice Hall, Pearson Education, Inc.

Mondal, P., Shah, S. P., Marks, L. D., & Gaitero, J. J. (2010). *Comparative Study of the Effects of Microsilica and Nanosilica in Concrete*. In *Transportation Research Record. Journal of the Transportation Research Board, n°. 2141* (pp. 6–9). Washington D.C.: Transportation Research Board of the National Academies.

Najigivi, A., Khaloo, A., Iraji zad, A., & Abdul Rashid, S. (2013). Investigating the effects of using different types of SiO_2 nanoparticles on the mechanical properties of binary blended concrete. *Composites: Part B, 54*, 52–58.

Nazari, A., & Riahi, S. (2010). Microstructural, thermal, physical and mechanical behavior of the self compacting concrete containing Si_2O nanoparticles. *Materials Science and Engineering A, 527*, 7663–7672.

Nazari, A., & Riahi, S. (2011a). Abrasion resistance of concrete containing SiO_2 and Al_2O_3 nanoparticles in different curing media. *Energy and Buildings, 43*, 2939–2946.

Nazari, A., & Riahi, S. (2011b). The effects of SiO_2 nanoparticles on physical and mechanical properties of high strength compacting concrete. *Composites: Part B, 42*, 570–578.

Oltulu, M., & Sahin, R. (2011). Single and combined effects of nano-SiO_2, nano-Al_2O_3 and nano-Fe_2O_3 powders on compressive strength and capillary permeability of cement mortar containing silica fume. *Materials Science and Engineering A, 528*, 7012–7019.

Oltulu, M., & Sahin, R. (2013). Effect of nano-SiO_2, nano-Al_2O_3 and nano-Fe_2O_3 powders on compressive strengths and capillary water absorption of cement mortar containing fly ash: a comparative study. *Energy and Buildings, 58*, 292–301.

Qing, Y., Zenan, Z., Deyu, K., & Rongshen, C. (2007). Influence of nano-SiO_2 addition on properties of hardened cement paste as compared with silica fume. *Construction and Building Materials, 21*, 539–545.

Quercia, G., Spiesz, P., Hüskenc, G., & Brouwers, H. J. H. (2014). SCC modification by use of amorphous nano-silica. *Cement & Concrete Composites, 45*, 69–81.

Rivera Lozano, J. (2004). *La hidratación de la pasta de cemento con adiciones activas* (Ph. D. thesis). Facultad de Ciencias, Universidad Autónoma de Madrid.

Sánchez, E., Garcimartín, M. A., Jofré, C., & Burón, M. (2010). *Manual para el empleo del hormigón en obras agrícolas*. Madrid. Spain: Instituto español del cemento y sus aplicaciones (IECA).

Sánchez, F., & Sobolev, K. (2010). Nanotechnology in concrete – a review. *Construction and Building Materials, 24*, 2060–2071.

Schmidt, M., Amrhein, K., Braun, T., Glotzbach, C., Kamaruddin, S., & Tänzer, R. (2013). Nanotechnological improvement of structural materials – impact on material performance and structural design. *Cement & Concrete Composites, 36*, 3–7.

Senff, L., Hotza, D., Repette, W. L., Ferreira, V. M., & Labrincha, J. A. (2010). Mortars with nano-SiO_2 and micro- SiO_2 investigated by experimental design. *Construction and Building Materials, 24*, 1432–1437.

Singh, L. P., Agarwal, S. K., Bhattacharyya, S. K., Sharma, U., & Ahalawat, S. (2011). Preparation of silica nanoparticles and its beneficial role in cementitious materials. *Nanomaterials and Nanotechnology, 1*(1), 44–51.

UNE 83982. (2008). *Determinación de la absorción de agua por capilaridad del hormigón endurecido*. Madrid. Spain: Asociación Española de Normalización y Certificación (AENOR).

UNE-10972. (2010). *Ensayos para determinar las propiedades mecánicas y físicas de los áridos. Parte 2: Métodos para la determinación de la resistencia a la fragmentación*. Madrid. Spain: Asociación Española de Normalización y Certificación (AENOR).

UNE-CEN/TS 12390 EX. (2008). *Ensayo de hormigón endurecido. Resistencia al hielo-deshielo. Pérdida de masa superficial*. Madrid. Spain: Asociación Española de Normalización y Certificación (AENOR).

UNE-EN 196-1. (2005). *Métodos de ensayos de cementos. Parte 1: Determinación de resistencias mecánicas*. Madrid. Spain: Asociación Española de Normalización y Certificación (AENOR).

UNE-EN 197-1. (2011). *Cemento. Parte 1: Composición, especificaciones y criterios de conformidad de los cementos comunes*. Madrid. Spain: Asociación Española de Normalización y Certificación (AENOR).

Zhang, M.-H., & Li, H. (2011). Pore structure and chloride permeability of concrete containing. *Construction and Building Materials, 25*, 608–616.

Zyganitidis, I., Stefanidou, M., Kalfagiannis, N., & Logothetidis, S. (2011). Nanomechanical characterization of cement-based pastes enriched with SiO_2 nanoparticles. *Materials Science and Engineering B, 176*, 1580–1584.